Forelimb force direction and magnitude independently controlled by spinal modules in the macaque

Amit Yaron[a,1], David Kowalski[a,b,1], Hiroaki Yaguchi[a,1], Tomohiko Takei[a,c], and Kazuhiko Seki[a,2]

[a]Department of Neurophysiology, National Institute of Neuroscience, Kodaira, 187-8502 Tokyo, Japan; [b]School of Biomedical Engineering, Science and Health Systems, Drexel University, Philadelphia, PA 19104; and [c]Graduate School of Medicine, The Hakubi Center for Advanced Research, Kyoto University, 606-8501 Kyoto, Japan

Edited by Peter L. Strick, University of Pittsburgh, Pittsburgh, PA, and approved September 4, 2020 (received for review November 6, 2019)

Modular organization of the spinal motor system is thought to reduce the cognitive complexity of simultaneously controlling the large number of muscles and joints in the human body. Although modular organization has been confirmed in the hindlimb control system of several animal species, it has yet to be established in the forelimb motor system or in primates. Expanding upon experiments originally performed in the frog lumbar spinal cord, we examined whether costimulation of two sites in the macaque monkey cervical spinal cord results in motor activity that is a simple linear sum of the responses evoked by stimulating each site individually. Similar to previous observations in the frog and rodent hindlimb, our analysis revealed that in most cases (77% of all pairs) the directions of the force fields elicited by costimulation were highly similar to those predicted by the simple linear sum of those elicited by stimulating each site individually. A comparable simple summation of electromyography (EMG) output, especially in the proximal muscles, suggested that this linear summation of force field direction was produced by a spinal neural mechanism whereby the forelimb motor output recruited by costimulation was also summed linearly. We further found that the force field magnitudes exhibited supralinear (amplified) summation, which was also observed in the EMG output of distal forelimb muscles, implying a novel feature of primate forelimb control. Overall, our observations support the idea that complex movements in the primate forelimb control system are made possible by flexibly combined spinal motor modules.

monkey | spinal cord | force field | summation | modularity

To execute voluntary movement, the central nervous system (CNS) must convert the desired movement into signals that control muscles and thus the actual position of the body in space. Large numbers of possible movements (i.e., large degrees of freedom, DOF), nonlinear dynamics, and sensory delays in the musculoskeletal apparatus make voluntary movements a computational challenge. How the CNS accomplishes this conversion is a long-standing question in the field of motor control. A hierarchical and modular organization of the CNS for controlling movement might simplify this process. In this scheme, a limited number of output modules in the spinal cord would control different but overlapping sets of muscles and joints, thereby decreasing the number of variables directly controlled by the cerebral cortex. By recruiting different output modules simultaneously but independently, the CNS might take advantage of this modular structure and achieve the flexibility necessary to control a variety of behaviors at a lower computational cost than is accrued by controlling each muscle independently (1–3). Bizzi and colleagues (1, 4, 5) pioneered the original experimental evaluation of this hypothesis, showing that hindlimb movement generated by costimulation (simultaneous stimulation) of two sites in the frog lumbar spinal cord could be explained by a simple linear sum of the responses evoked by stimulating each site individually. Based on this seminal work, they further hypothesized that the supraspinal structure might control the large number of DOF by activating and combining different motor "modules" in the spinal cord (3, 6, 7). Subsequent work in the frog (8–10), rodent (11, 12), and cat (13) confirmed these results. In this paper, we tested whether the same scheme exists in the primate forelimb-control system.

Today, the concept of modular organization is used as a basis in studies of human movement (14, 15). Indeed, a number of different human joint movements and muscle activities have been characterized based on this idea (i.e., muscle synergy) (16, 17), and it has even spread to fields of clinical research (18, 19) and robotic engineering (20–22). Although these studies implicitly assume that the concept of modular motor control derived from frogs and small mammals also applies to humans, few studies have attempted to directly determine whether such control is present in the primate spinal circuitry. We recently reported that cervical spinal interneurons in monkeys coactivate multiple finger muscles (23) with several time-varying profiles (24) and that these coactivations could correspond to muscle synergies in primate hand muscles (25). These findings seem to support the idea that primate forelimb movement is also controlled through modular organization and raise the possibility that efficient control of the primate limb is accomplished via brain activation of different sets of spinal cord modules (26, but see refs. 27 and 28), as previously seen in the legs of frogs (5) and rodents (11).

To test this idea, we reproduced the original experimental paradigm in the cervical spinal cord (for control of forelimbs rather than hindlimbs) of anesthetized monkeys, measuring the direction and magnitude of the force field generated by

Significance

Studies in frogs and rodents have shown that to deal with the complexity of controlling all the muscles in the body the brain can activate sets of neurons in the spinal cord with a single signal. Here, we provide confirmation of a similar system of "modular" output in nonhuman primates. Costimulation at two spinal sites resulted in force field directionality that was the linear sum of the fields from each site. However, unlike the frog and rodent, the magnitude of the force vectors was greater than the simple sum (supralinear). Thus, while force direction in primates is controlled by the linear sum of modular output, force amplitude might be adjusted by additional sources shared by those modules.

Author contributions: D.K. and K.S. designed research; D.K., H.Y., and T.T. performed research; A.Y. and D.K. analyzed data; and A.Y., D.K., H.Y., T.T., and K.S. wrote the paper.

The authors declare no competing interest.

This article is a PNAS Direct Submission.

[1]A.Y., D.K., and H.Y. contributed equally to this work.

[2]To whom correspondence may be addressed. Email: seki@ncnp.go.jp.

This article contains supporting information online at https://www.pnas.org/lookup/suppl/doi:10.1073/pnas.1919253117/-/DCSupplemental.

costimulation as well as the electromyography (EMG) output (1, 4, 5). We tested the effect of electrically stimulating pairs of intraspinal sites both individually and simultaneously by comparing the evoked force fields measured at the wrist joint as well as the activity of several forelimb muscles. As in the lumbar spinal cord of other species (5, 11, 12), we found that the directionality of the force field evoked after simultaneous stimulation could be explained by linearly summing the force fields generated when each intraspinal site was stimulated separately. We further confirmed a comparable linear summation in the EMG output of proximal forelimb muscles as the potential source of the force fields' linear summation. Additionally, we unexpectedly found supralinear facilitation of force field magnitude, which has not been reported in previous studies. We discuss a potential source and functional significance of this supralinear facilitation.

Results

Force Patterns Evoked by Coactivation of Two Intraspinal Sites Show Linear Summation in Direction. Previous research on the frog spinal cord (1, 4, 5) has shown that costimulation of two spinal cord sites results in a force field that is the simple linear sum of the fields evoked when each site is stimulated individually. To determine if these effects are also seen in primates, here we examined isometrically measured X–Y force responses at the wrist in seven different hand positions that were induced by microstimulation of the monkey spinal cord (Fig. 1 *A–D*). This allowed us to obtain the force fields associated with each intraspinal site (Fig. 1 *E* and *F*).

An example of force fields evoked by an electrode pair (monkey TE, 4-mm depth) is shown in Fig. 2 *A–D*. When analyzing the direction of the observed resultant force fields from the costimulation of this pair of intraspinal sites (Fig. 2*D*, F_{Ob}), we found that although it did not match the field resulting from stimulation of either site individually (Fig. 2 *A* and *B*, F_A, cosine similarity = 0.63; F_B, similarity = 0.76), it was closely predicted by the field expected by simple summation of the two (Fig. 2*C*, F_{Ex}, similarity = 0.91; similarities summarized in Fig. 2*E*). Across all costimulations, we found that the similarity between force fields observed after costimulation and those predicted by the linear sum was high (>0.90) in 77% (23/30) of intraspinal site combinations and that the average similarity for all 30 cases was 0.92 ± 0.015 (SE). While in many of the cases [16/30 here and 24/41 in the frog (5)], the response to costimulation was highly similar (>0.90) to the response to stimulation at one of the individual sites, in most cases [24/30 here and 33/41 in the frog (5); Fig. 2*F*] the force fields elicited by costimulation were more similar to the linear combination of the two evoked fields than to either individual evoked field. Importantly, this was true for both the "winner" and "loser" sites ("winner" similarity: 0.85 ± 0.03; "loser" similarity: 0.58 ± 0.06; $P < 0.005$ for both comparisons). For comparison, the similarity between the costimulation field and the linear sum of the component fields in the frog (5) was 0.938 ± 0.045, while that of the "winner" site was 0.905 ± 0.068. Therefore, the force field directionality produced by simultaneous spinal-site stimulation can be explained by linearly summing the force fields generated by each site. This replication of past findings in other species suggests that primate forelimb control is accomplished by the flexible combination of spinal cord modules.

Muscle Responses Also Show Linear Summation. The underlying assumption of the proposal that modular organization is based on the linear sum of force field directionality is that the force vectors represent spinal recruitment of motor output. Thus, a given spinal locus generates its force vector output by recruiting and/or changing the activity of (a set of) muscle(s), generating torques at the shoulder and elbow, and creating a measurable force at the wrist. If so, our linear-summation findings imply that (at least) two intraspinal loci can concurrently and independently recruit sets of muscle fibers representing different force field directions.

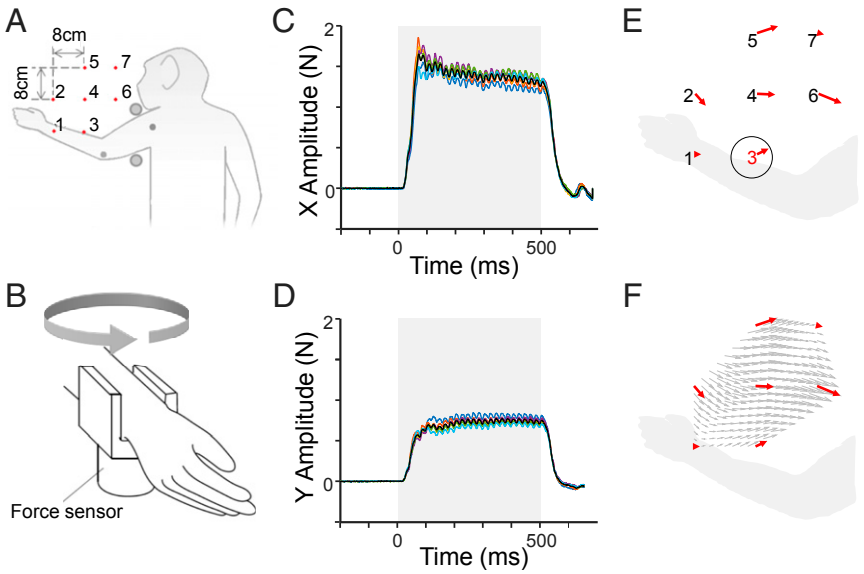

Fig. 1. Method for measuring force fields. (*A*) A monkey was anesthetized and laid prone on a horizontal table. The posture of the left limb was changed by manually fixing the left wrist at one of seven points on a square grid with 8-cm spacing (red dots). The shoulder was stabilized with two vertical poles (gray circles) [adapted from Yaguchi et al. (60)]. (*B*) The wrist was fixed at each point using a swiveling U-shaped hand holder with an integrated force sensor. (*C* and *D*) The forces recorded in the mediolateral (or X) (*C*) and anteroposterior (or Y) (*D*) directions during stimulation (gray shades) of a specific intraspinal site (or combination) at a specific hand position. The colored lines each represent the measured force during a single pulse train; the black line is the mean force response over multiple trials ($n = 6$). (*E*) The magnitude and direction of the force vector in the X–Y plane at a single location were determined by finding the total area of force magnitude and its corresponding direction. The black circle shows the location at which the force vectors were obtained for the example in *C* and *D*. (*F*) The estimated force field from *E* was further visualized by interpolation.

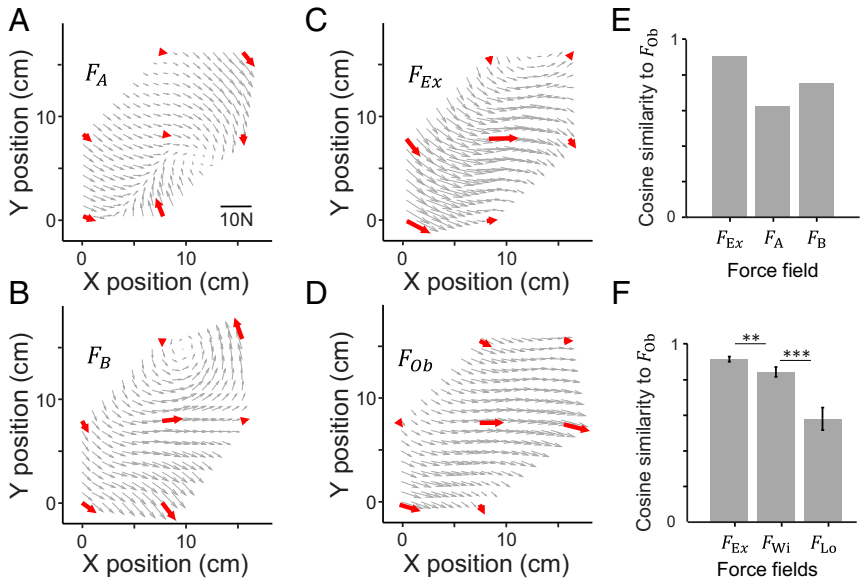

Fig. 2. A representative example of the linear sum of force fields evoked by microstimulating pairs of intraspinal sites. (*A* and *B*) Force patterns evoked by stimulating two intraspinal sites (A, site 2 and B, site 11, monkey TE, 4-mm depth). Note that the vector profiles of the force fields (F_A and F_B) are different. (*C*) Expected output (F_{Ex}) based on the assumed linear summation of F_A and F_B. (*D*) Actual observed field (F_{Ob}) evoked by stimulating sites A and B simultaneously (costimulation). Red arrows illustrate the measured force vectors at seven different wrist positions and black arrows show the interpolated vectors, giving a smoother visualization of the forces. (*E*) Similarity for a representative example. Bars indicate the cosine similarity that the field resulting from costimulation (*D*) had with those generated at site A (A, F_A) and B (B, F_B) and with their linear combination (C, F_{Ex}). The SI, in this case, was −0.16. (*F*) Similarity for the population (n = 30 site parings). Bars indicate the mean (± SE) cosine similarity that the fields resulting from costimulation had with those generated at "winner" sites (F_{Wi}, the sites that had the higher similarity of the two individually stimulated sites) and at "loser" sites (F_{Lo}, the sites that had the lower similarity), and with the field expected by their linear combinations (F_{ex}). $^{**}P < 0.001$, $^{***}P < 0.0001$.

To test this possibility, we first compared force vector responses with simultaneously evoked EMG responses in 185 intraspinal site–muscle pairs that exhibited significant (>3× SD of the background signal; *see Methods*) EMG responses for a given muscle at all seven wrist positions. An example is shown in Fig. 3 *A*–*C*. In this example (elbow muscle, lateral head of the triceps brachii [TLA]; Fig. 3*B*), the magnitude of the responses varied among the different arm configurations. Furthermore, the mean EMG amplitude seemed to covary with the force direction (Fig. 3*A*). Indeed, we found a significant correlation between force vector direction and EMG magnitude (Fig. 3*C*; $r = 0.89$, $P < 0.05$). We analyzed all 185 intraspinal site-muscle pairs, and the results are summarized in Fig. 3*D*. We found that the degree of correlation varied across muscles, with the highest correlations in an elbow extensor (TLA) and a shoulder extensor (spinal deltoid, DES) (hereafter referred to as the "top-two" muscles) and smaller correlations in the finger and wrist muscles. Making the same comparison between different groups of muscles, we found that force direction was highly correlated with EMG magnitude for elbow and shoulder muscles and significantly less so for wrist and finger muscles ($P < 0.05$). The correlation for the top-two muscles (black bar, Fig. 3*E*) was significantly higher than that for the other shoulder and elbow muscles ($P < 0.05$). Therefore, we can conclude that force field directionality as measured at the wrist in this study was generated predominantly by the elbow and shoulder muscles, rather than the wrist and finger muscles. This result is corroborated by anatomical evidence that the shoulder and elbow muscles are the prime contributors to end-point force at the wrist, although the wrist muscles also can act synergistically with elbow muscles to influence motor output (29, 30).

Having confirmed that elbow and shoulder muscles were driving force field directionality when stimulating a single site, we tested whether costimulation generated total motor output that was a linear sum of individual motor outputs. We selected costimulation site pairs from the site–muscle pairings used in Fig. 3 and computed the EMG vectors (two individual and one costimulation; *see Methods*) among the different muscle groups (all 12 muscles, wrist/finger set, elbow set, shoulder set, and the top-two muscles; Fig. 3*E*). We then compared the cosine similarity for these vectors (i.e., costimulation EMG vs. the linear sum of single-site EMGs) with the cosine similarities observed for the force fields. An example of this EMG vector analysis is shown in Fig. 4 *A*–*D*. Single-site stimulation of two intraspinal loci evoked a significant response in a shoulder (DES) and an elbow (TLA) muscle (the top-two group) with different magnitudes (Fig. 4 *A* and *B*). A two-dimensional representation of the vector space highlighting the activity of these two muscles can be seen in Fig. 4*C*, with the linear sum of the EMG vectors for site A (blue) and site B (cyan) represented in orange. We then compared the observed EMG vector after costimulation at these two locations (red in Fig. 4*D*) with the linear sum (orange in Fig. 4 *C* and *D*). For this particular pair of sites, the cosine similarity for the EMG vector was 0.94. A similar analysis, done in multidimensional space (according to the number of muscles in each group), was repeated for the 185 intraspinal site–muscle group pairs, and the results are summarized according to each muscle group (Fig. 4*E*).

Because the EMG magnitude measure used in our vector analysis is always nonnegative, EMG vector direction is restricted. Determining whether the calculated cosine similarity between the costimulated EMG vector field and its individual site components is greater than chance levels is thus critical. Importantly, the level of chance similarity may depend on the number of muscles included in the vector. Therefore, in addition to the actual cosine similarity, we also calculated the chance-level similarity for random groupings of equal numbers of muscles. We then used these chance levels to correct the overall

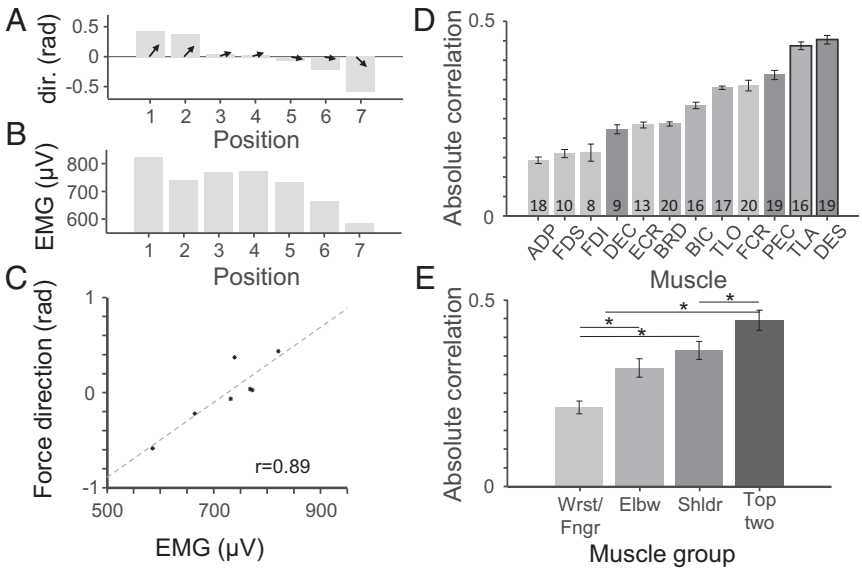

Fig. 3. Correlation of EMG responses with force direction. (*A*) An example of force direction measured in monkey TE in response to stimulation of intraspinal site 2 (depth: 4 mm) at seven hand positions, ordered by the force vector direction (positions 3, 6, 1, 4, 2, 5, and 7 from Fig. 1*A*. Arrows illustrate the direction; bars represent the direction in radians (with east as 0). (*B*) An example of average rectified EMG amplitude from the lateral head of the triceps brachii (TLA) over the stimulation period, recorded at the same time as the force in *A*. (*C*) The direction of the force vector (*A*) and the EMG response amplitude (*B*) were significantly and positively correlated ($r = 0.89$, $P < 0.05$). (*D*) The mean (± SE) of the absolute correlation coefficients between the mean EMG amplitudes in response to stimulation at a single intraspinal site and the directions of the simultaneously induced force vectors, computed for each muscle. The numbers at the base of each bar are the number of relevant combinations found for each muscle across all intraspinal stimulation sites and hand positions, where a significant response (rectified EMG amplitude surpassed 3× SD) in all seven positions was required to be included in this test. (*E*) Same data as *D*, divided into groups of related muscles (number of muscles in each group indicated). *$P < 0.05$.

muscle group similarity measures, thus accounting for the different number of muscles in each group when determining statistical significance (*Methods*).

We found that cosine similarity was highest for the TLA and DES muscle-pair group (top-two similarity: 0.91 ± 0.02 SE; mean chance similarity: 0.29), followed by the significantly lower shoulder-muscle group (similarity: 0.75 ± 0.03; chance level: 0.26; vs. top-two and corrected for different chance levels: $P < 0.01$). The similarities were even lower in the elbow- (similarity: 0.5 ± 0.05; chance level: 0.25) and wrist/finger-muscle groups (similarity: 0.5 ± 0.05; chance level: 0.24), both of which were significantly lower than that in the shoulder-muscle group ($P < 0.05$ for both). The lowest computed similarity (but still significantly higher than chance) used EMG vectors representing all muscles (similarity: 0.44 ± 0.06; chance level: 0.23). The cosine similarity for the top-two muscle group was comparable to that for the force field directionality (Fig. 2 and Table 1; 0.91 ± 0.02 vs. 0.92 ± 0.015, $P > 0.05$). Importantly, all cosine-similarity measures for the costimulated EMG vector fields were significantly higher than the chance level of similarity for the number of muscles included in the vector. Furthermore, as with the force field analysis, we compared the similarity for the top-two EMG vector field during costimulation (E_{Ex}) with those for the fields generated when each site was stimulated separately (Fig. 4*F*). We found that the mean similarity for both "winner" sites (E_{Wi}, 0.84 ± 0.03) and "loser" sites (E_{Lo}, 0.65 ± 0.04) was lower than the similarity between the observed and linear-sum expectation for costimulation (0.9 ± 0.02, paired *t* test, $P < 0.05$ and $P < 0.005$, respectively). Based on the results depicted in Figs. 3 and 4, we conclude that the force field elicited by costimulation is highly similar to the linear sum (Figs. 2 and 4 *E* and *F* and Table 1) because it arises predominantly through the linear summation of EMG vectors for the muscles that contribute the most in shaping the force field direction (in this case, the shoulder muscles and the elbow extensor). This result also suggests that the cosine similarity for the observed costimulation force field direction indeed represents a physiological process in the spinal cord that shapes the balance within the specific muscle sets so that it best fits the motor plan (i.e., direction). Furthermore, these findings support the idea that a large variety of motor outputs can be achieved via a linear combination of spinal motor modules (2, 3, 29, 31), which has recently been suggested to occur in primate proximal muscles (32) and confirmed in primate distal muscles (25).

Supralinear Summation in Force Field Magnitude. A force field can be characterized by the directions and magnitudes of its component vectors (4, 5). We have thus far shown that the directionality of a field produced by costimulation can be predicted from the simple linear summation of the component fields and that the underlying mechanism can likewise depend on the summation of muscle-group activity (synergies). In addition to direction, we also examined force field magnitude using nonnormalized force vectors, as shown in Fig. 5 *A* and *D*. For this example pair of intraspinal stimulation sites, although the vector's direction after costimulation (red arrow) resembled the linear sum (orange) of individual vectors during single stimulations (blue and cyan), we found that the vector's magnitude after costimulation was far larger than the simple linear sum (six times larger). Had all of the vectors in this resultant field displayed the same facilitation, the scaling coefficient, *c* (*Methods*), would have also been 6, suggesting that costimulation leads to supralinear facilitation of force field magnitude. Across all costimulations, the vector scaling coefficient ranged from 0.019 to 152.4, with a value of 1 indicating an exact linear summation. To have a less skewed measure of facilitation (or depression), we defined a scaling index (SI) as the natural logarithm of *c* (with a value of 0 now representing a simple linear summation). In this case, a *c* of 6 corresponds to an SI of 1.8. A similar comparison was made for all 123 cases summarized in Fig. 5 *G*, *Left*. The mean SI was

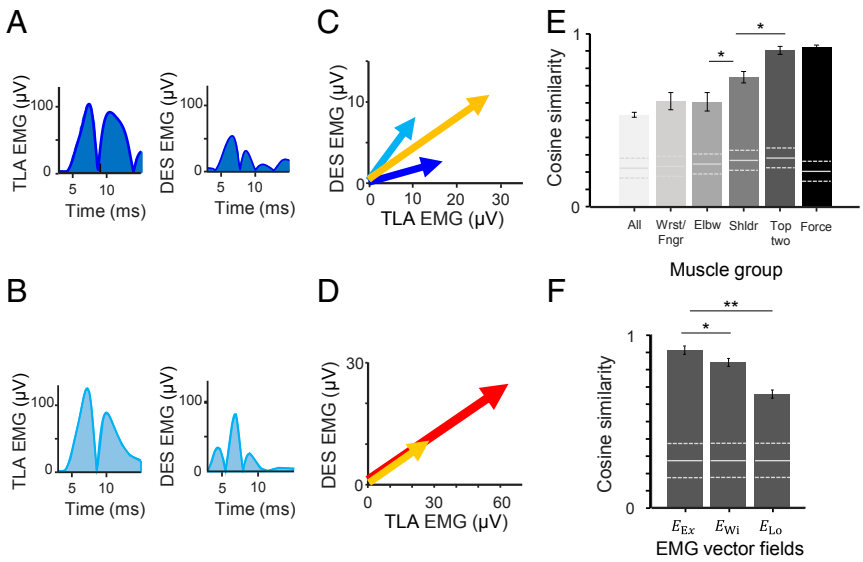

Fig. 4. Linear summation in the direction of EMG vectors. (*A* and *B*) An example of EMG responses simultaneously evoked in the lateral head of the triceps brachii (TLA, *Left*) and spinal part of the deltoid (DES, *Right*) of monkey NE in response to stimulation with the wrist in the third position (Fig. 1*A*). Response to stimulation applied at different intraspinal sites is presented in *A* and *B* (*A*: intraspinal site 10, depth: 2 mm; *B*: intraspinal site 28, depth: 2 mm). Note that for visual clarity only the response to the first pulse in the stimulus train is presented. (*C*) EMG vectors calculated from the EMG response shown in *A* (blue) and *B* (cyan), and the linear sum of the two (orange). (*D*) EMG vectors obtained from EMG responses of both muscles during costimulation (red) and the expected linear-sum vector (orange, same as in *C*). Note that the directions of actual and expected EMG vectors are highly similar. Cosine similarity = 0.99, SI = 0.84. (*E*) Mean (± SE) of the cosine similarity between the EMG vectors generated by costimulation and those expected by linear summation, computed for each group of muscles. Cosine similarity calculated from the force fields (Fig. 2 and Table 1) is shown for comparison. Gray lines indicate chance level similarity and dashed lines indicate the 95th and 5th percentiles of the distribution. (*F*) Mean (± SE) cosine similarity for muscles TLA and DES between fields generated by costimulation and single stimulation of "winner" sites (E_{Wi}, the sites with the higher similarity of the two), "loser" sites (E_{Lo}, the sites with the lower similarity), and the linear combinations (E_{Ex}). $*P < 0.05$; $**P < 0.001$.

1.54 ± 0.12 (SE), suggesting that on average costimulation resulted in a force magnitude 4.7 times that expected by the linear sum [compared to 0.88 on average in the original experiments in the frog (5)].

The supralinear summation of force field magnitude suggests that the motor output from two intraspinal sites might be integrated and magnified by shared premotor systems, a process commonly known as "spatial facilitation" (33). To address this possibility, we performed a similar analysis, computing SIs for the EMG vectors by comparing the magnitudes of EMG responses for each muscle between single- and costimulation conditions. Fig. 5 *B* and *C* present examples for the flexor carpi radialis (FCR, wrist muscle) and TLA (elbow muscle), respectively. While the EMG magnitude during costimulation was similar to the linear sum (SI = −0.19) in the elbow muscle (Fig. 5 Fig. *C* and *F*), that in the wrist muscle (Fig. 5 *B* and *E*) was much larger (SI = 1.86; supralinear summation). We performed this analysis for 210 intraspinal site–muscle combinations (Fig. 5 *G* and *H*). The average SI for a vector containing all 12 muscles was 0.59 ± 0.11 (corresponding to 1.8-fold facilitation), suggesting

Table 1. Comparison with earlier studies

	This paper	Mussa-Ivaldi et al. (5)	Tresch and Bizzi (11)	Lemay et al. (34)	Caggiano et al. (12)
Animal	Monkey	Frog	Rat	Cat	Mouse
Limb	Arm	Leg	Leg	Leg	Leg
Spinal segment	Cervical	Lumbar	Lumbar	Lumbar	Lumbar
Stimulation	Electrical	Electrical	Electrical	Electrical	Electrical
Side	Ipsilateral	Ipsilateral	Ipsilateral	Contralateral (4) and ipsilateral (2)	Ipsilateral
Preparation	Intact	Spinalized (acute)	Spinalized (chronic)	Decerebrated (acute)	Intact
Anesthesia	Ketamine and medetomidine	n.a.	n.a.	n.a.	Ketamine and xylazine
Similar to linear sum	25/30 (83%)	36/41 (86%)	6/7 (86%)	0/6 (0%)	27/31 (87.1%) chat 45/58 (77.6%) thy1
Average directional similarity	0.9 ± 0.041	0.938 ± 0.045	n.a.	n.a.	0.90 ± 0.05 chat 0.86 ± 0.10 thy1
Facilitation	2.65 ± 1.3	1.08 ± 0.4	Not specified	1.26 ± 0.81	0.84–1.37 (from Figs. 5 and 6)

n.a., data not available in the comparison paper.

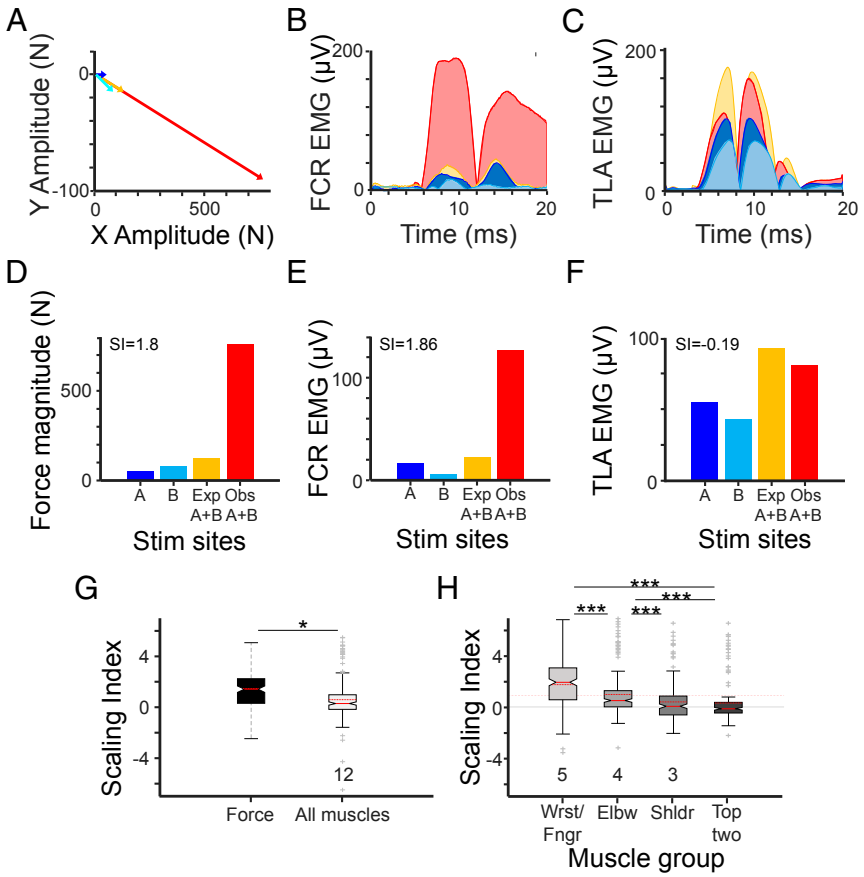

Fig. 5. Summation of force field magnitude and EMG vector magnitude. (*A*) Examples of force vectors evoked by the stimulation at two sites separately (blue, intraspinal site 1, depth: 3 mm; cyan, site 14, depth: 3 mm) and the costimulation (red) are displayed together with the expected response assuming a simple linear sum (orange). The bar plot for each panel represents the force magnitude for each. Note the supralinear summation (facilitation) in the magnitude (SI = 0.7158) while the direction of the force vector matches the expected linear sum. (*B* and *C*) Examples of the EMG responses that were simultaneously measured with the force field shown in *A*. The same color scheme is used for each line and bar plot. An example of the wrist muscle (*B*, FCR) and an example of the elbow muscle (*C*, lateral head of the triceps brachii [TLA]) are shown. Both examples were recorded in the third position (Fig. 1*A*) from monkey NE. (*D*) The bar plot represents the force magnitude for each site and the combinations using the same color scheme in *A*. Note the supralinear summation (facilitation) in the magnitude (SI = 1.8 [$c = 6.05$]) while the direction of the force vector matches the expected linear sum. (*E* and *F*) The bar plots represent the area of responses over all stimulus trains for the FCR (*E*) and TLA (*F*). Note that the actual and expected EMG vector magnitudes are comparable for the elbow muscle (*F*) (SI = −0.19, c = 0.83) but not for the wrist muscle (*E*) (SI = 1.86, $c = 0.83$) (see Fig. 4). (*G*) Box plot showing the distribution of force-scaling indexes (*Left*; the contrast in force between the magnitude of responses to paired and unpaired stimulation) or EMG-scaling indexes (*Right*; the contrast between vector magnitudes for all muscle responses to paired and unpaired stimulation), for all monkeys, days, and positions ($n = 123$ for force, mean SI = 0.976, mean $c = 2.65$; $n = 210$ for EMG, mean SI = 0.59, mean $c = 1.8$). (*H*) Box plot showing the distribution of EMG SIs for different muscle groups [the contrast between response-vector magnitudes for muscles in different groups to paired and unpaired stimulation for all intraspinal sites and positions ($n = 748$)]. The details for the groups are as follows. Wrist/shoulder muscles: five muscles, $n = 209$, mean SI = 1.78, mean $c = 5.9$; elbow muscles: four muscles, $n = 207$, mean SI =1.0, mean $c = 2.73$; shoulder muscles: three muscles, $n = 158$, mean SI = 0.41, mean $c = 1.51$; top-two muscles: $n = 158$, mean SI = 0.34, mean $c = 1.4$. For both *G* and *H*, the boxes are centered on the median of the distribution (red line) and its top and bottom edges indicate the 25th and 75th percentiles of the distribution. The dashed red line represents the mean. Outliers are marked by + signs, and the whiskers show the extent of all data that are not considered outliers. The notches represent 5% confidence intervals around the medians. $*P < 0.05$; $***P < 0.0001$.

that muscle responses also show supralinear summation, albeit smaller than that of force field magnitude (Fig. 5*D*). Next, we compared the magnitude of the EMG vector for each group of muscles, similar to what is seen in Fig. 4*E*. As shown in the example (Fig. 5 *B* and *E* and Fig. 5 *C* and *F*), we found a significant difference among the muscle groups. The SI for the wrist and finger muscles (1.8 ± 0.13, 5.9-fold facilitation) was significantly larger than that for the elbow (1 ± 0.11, $P < 0.001$). Shoulder muscles (0.41 ± 0.12, $P < 0.001$) as well as muscles whose contributions dominated the force field direction (top-two in Fig. 3*E*, 0.34 ± 0.13, $P < 0.001$) showed significantly smaller SIs than those from other groups. Indeed, the median SI in the top-two- and shoulder-muscle groups was close to zero (top-two: −0.11; shoulder: 0.09), suggesting that summation for response magnitude in the proximal muscles was almost linear. Comparing the SI for each muscle group with that for the force field magnitude (mean = 0.96, red horizontal line in Fig. 5*H*) indicated that elbow- and shoulder-muscle SIs were comparable, but that the SI for the wrist/finger muscles was much larger than that for the force field magnitude.

The results described in Fig. 5 can be summarized as follows. First, supralinear summation observed in the force field magnitude was confirmed in the EMG vectors. Second, the extent of supralinear summation in the EMG vector fields differed depending on the muscle group; it was larger in distal muscles and smaller in proximal muscles. Third, when present, supralinearity for the proximal muscles was comparable to or smaller than that for force magnitude.

Given the low SI for the proximal muscles (nearly linear, Fig. 5*H*), one may wonder how a supralinear summation in the

force field magnitude (Fig. 5*G*) was generated, because we have shown that the elbow and shoulder muscles were driving force field direction (Fig. 3). This question can be addressed by making a direct comparison between the SIs of the costimulated force fields and those of the EMGs, similar to what is shown in Fig. 3. An example is shown in *SI Appendix*, Fig. S1 *A–C*. In this example (elbow muscle TLA; *SI Appendix*, Fig. S1*B*), the SI for the responses varied among the different arm configurations. Furthermore, for this specific muscle, the mean EMG amplitude seemed to covary with the force SI (*SI Appendix*, Fig. S1*A*). Indeed, we found a significant correlation between force vector SI and EMG SI (*SI Appendix*, Fig. S6*C*; $r = 0.7$, $P < 0.05$). We analyzed all 110 intraspinal site combinations of muscle pairs and summarize the results in *SI Appendix*, Fig. S1*D*. We found that the degree of correlation varied across muscles, with the top-two muscles (i.e., TLA and DES) among the highest three correlations (*SI Appendix*, Fig. S1*D*). Making the same comparisons between different groups of muscles, we found that the SIs for force magnitude and EMG magnitude were highly correlated with each other in the top-two and elbow-muscle groups, and the degrees of correlation for these two groups were significantly higher than what was observed for the wrist/finger muscles ($P < 0.01$ and $P < 0.05$, respectively). Therefore, the supralinear summation of force field magnitude might be ascribed to the supralinear summation of EMG output from primarily proximal muscles, even if their individual EMG SIs were smaller than those of the distal muscles.

Other Factors That May Influence the Direction and Magnitude of Force Fields and Their Summation. Unlike the original experiments in frogs and smaller mammals, in monkeys we found that even though muscle output, and thus the magnitude of the force field, could be modified during costimulation, EMG unit vectors (representing possible motor synergies) and the direction of the output force fields were often maintained. To ensure that our measurements were not the result of artifacts created by our experimental setup, we examined whether electrode depth (*SI Appendix*, *Supplementary Information Text* and Fig. S2), stimulus current (*SI Appendix*, *Supplementary Information Text*), wrist position in the workspace (*SI Appendix*, *Supplementary Information Text* and Fig. S3), reafference signal from the hand and fingers (*SI Appendix*, *Supplementary Information Text* and Fig. S4), prior stimulation history (*SI Appendix*, *Supplementary Information Text* and Fig. S5), and the depth of anesthesia (*SI Appendix*, *Supplementary Information Text* and Fig. S6) affected the recruited fields and the system's response to costimulation. As we found that none of these factors showed systematic influence on the recruited field and responses to costimulation, we concluded that both the linear summation of the directionality as well as the supralinear summation of the magnitude could be unique properties of the primate cervical spinal cord.

Discussion

In this study, we measured the isometric wrist end-point force fields evoked by microstimulation delivered simultaneously to two discrete sites (costimulation) in the primate cervical spinal cord and compared them with those evoked by stimulating each site independently. We found that the direction of force fields generated by costimulation can be explained by the linear sum of those generated by independent stimulation (Figs. 2 and 4), with a comparable linear summation in the EMG vectors of the shoulder and elbow muscles (Figs. 3 and 4). In contrast, the magnitude of the force fields averaged 2.6 times greater than what was predicted by a simple linear summation (Fig. 5). While we found an increase in motor output from the elbow and shoulder muscles, the distal muscles in particular showed supralinear facilitation of output during costimulation. (Fig. 5). Interestingly, the two muscles with the highest synergistic similarity during costimulation (DES and TLA) also showed a near-linear summation of EMG-measured activity. Based on the observed linear sum of directionality in both EMG vector field and force output field, these results suggest that primate forelimb control could be achieved by combining multiple spinal cord modules, represented in the current study as the motor activity evoked by individual intraspinal site electrical stimulation.

This confirmation in the primate cervical spinal cord of the original results found in the lumbar cord of frog (1, 4, 5) and other species, despite several differences in the experimental setup (Table 1), strongly suggests that the control of limb movements by the flexible combination of spinal modules is robustly conserved in the cervical and lumbar spinal cord of most vertebrates, and therefore possibly in humans. The supralinear summation of motor output magnitude during costimulation, which has never before been reported, could be a unique feature of cervical spinal cord control in primates.

Linear Summation of Force Field Direction: Comparison with Earlier Studies. The primary motivation for this experiment was to reproduce in the monkey the original findings from the frog, as reported by Bizzi and colleagues (1, 4, 5): The force field recruited by costimulation of spinal loci is a simple vector sum of the two independently recruited force fields from those same sites. To discuss the possibility that the control of forelimb movement in monkeys, and therefore possibly higher primates, is also achieved by the flexible combination of spinal motor modules, we constructed an experimental setup that was comparable to the original study, including similar stimulus parameters for evoking end-point force vectors.

Based on the observed force field output, we reached a conclusion similar to that of the original investigation in the frog spinal cord (1, 4, 5): Fields evoked by costimulation are highly likely to be similar to the linear summation of the two individual fields (here, 77%, similarity index >0.9). In Table 1, we summarize the results and experimental setups of the earlier reports. Remarkably, high directional similarity has been reported in studies using several different species, including frogs (5), mice (12), rats (11), and monkeys (this study) despite variation in experimental protocols. For example, stimulation has been optical (12) or electrical (5, 11) (this study), the stimulated location has been in the cervical (this study) or lumbar (5, 11, 12) parts of the spinal cord, and animals have been anesthetized (12) (this study), acutely spinalized (5), or chronically spinalized (11). The consistent finding among these various experimental conditions that costimulation yields force directions that are highly similar to the linear sum of the component fields strongly supports the idea that a flexible combination of spinal modules for controlling movement is conserved throughout (at least) higher vertebrates. These findings in the cervical spinal cord mean that, rather than being confined to the hindlimb, this modular control could be a general feature of the forelimb and/or necessary for complex action sequences such as target reaching or throwing.

One exception is the report on the cat lumbar spinal cord, which found no cases (0/6) of directional linear summation during costimulation (34). However, in addition to the ipsilateral side, the intraspinal stimuli in that study were also applied to the contralateral side in four of six spinal cords. In contrast, stimulation in all of the other studies was limited to the ipsilateral side. Direct interaction between the sides of the spinal cord (35) is a well-known function of commissural interneurons (36). Therefore, the finding by Lemay et al. (34) might suggest that directional control of limb output force by linearly summing the component force field directions represented by multiple intraspinal sites could be restricted to unilateral, but not bilateral, control of force output.

Linear Summation of Force Field Direction: The Link with EMG Field Direction and Muscle Synergy. We also found a link between force vector direction and its corresponding EMG amplitude vector (Figs. 3 and 4), consistent with earlier reports in the lumbar spinal cord (11, 37, 38). Confirmation of this link in the cervical cord is crucial because it suggests that the linear sum of force field direction is a consequence of activity in the neural correlates of muscle synergy (31), as illustrated in Fig. 6. Here, let us assume that different force fields are produced by two different sets of motoneurons/muscles and that their excitability is regulated by excitatory premotor interneurons (12, 23–25, 39, 40). Stimulating the axon (either ascending or descending) that projects to a premotor interneuron (INa) recruits a group (synergy) of motoneurons/muscles (Syn-a) (25, 40) (A). This muscle synergy creates a specific EMG balance within the recruited muscles that is represented as the EMG vector (EVa). A given EMG vector should then be transformed into the force vector (FVa) via joint torque. This step is supported by our finding that the link between force and EMG vector field was dominant in the proximal muscles and that this link was the prime factor in determining the end-point force at the wrist (Fig. 3). Therefore, the correlation we found between FVa and EVa (Fig. 3) suggests that the force field direction evoked from a single intraspinal site could reflect the muscle synergy of proximal muscles that is likely represented by local premotor INs (25, 39, 40).

When two sites are activated simultaneously (Fig. 6*B*), the two sets of premotor neurons (INa and INb) representing two muscle synergies (Syn-a and Syn-b) and their EMG vectors (EVa and EVb) are recruited simultaneously. As we saw in Fig. 4, in some cases, the EMG vector generated by costimulation (EVab) is predicted by the linear sum of two component EMG vectors (EVa + EVb), suggesting that the two EMG vectors were summed linearly to generate the EMG vector during coactivation. Consequently, the link between the force field and EMG field during costimulation indicates that the linear sum of force field directionality during coactivation of two intraspinal sites reported in this paper and others reflects the recruitment of spinal interneurons that represent muscle synergies.

Finally, the link between end-point force direction and EMG vector direction was found predominantly in the proximal (mainly shoulder) muscles (Figs. 3 *D* and *E* and 4*E*). A similar link has been also reported in the proximal muscles of the hindlimb (hip flexor and extensor) (4, 11). Therefore, modular control of the spinal motor output is likely a shared feature for controlling proximal muscle activity of both arm and leg movements for most vertebrate species.

Linear Summation of Force Field Direction: Functional Significance. The significance of our findings in the primate cervical spinal cord is threefold. First, it confirms the possibility that, as hypothesized, spinal motor modules are indeed the building blocks for constructing movements (2, 7, 39) in primates. Previously, we found that spinal interneurons could coactivate a functionally relevant set of hand muscles (23) with a relevant firing pattern (24) and that they could be a part of the neural substrate for hand muscle synergies (25). Those results strongly supported the idea that primate spinal interneurons might serve as control modules for constructing activity from multiple muscles during voluntary movement. Here, by finding the linear summation of force field direction during costimulation, we can now suggest that primate limb movement is controlled by a flexible combination of spinal motor modules, which are represented by sets of premotor interneurons. Second, our findings on the modular control of motor output in the cervical spinal cord suggest that a variety of hand and arm movements can be constructed in the same manner (16, 32). A hallmark of modular organization in the motor system is that it would reduce the DOF required to control multiple muscles. Although this hypothesis has been examined exclusively in the hindlimb, the reduction in DOF should also benefit the control of the primate forelimb, allowing more complex movements at a lower computational cost. Noteworthily, we found linear summation of motor output, as evidenced by a vector analysis of the EMG signal (*Methods*), in both the distal and proximal muscles of the forelimb, with the

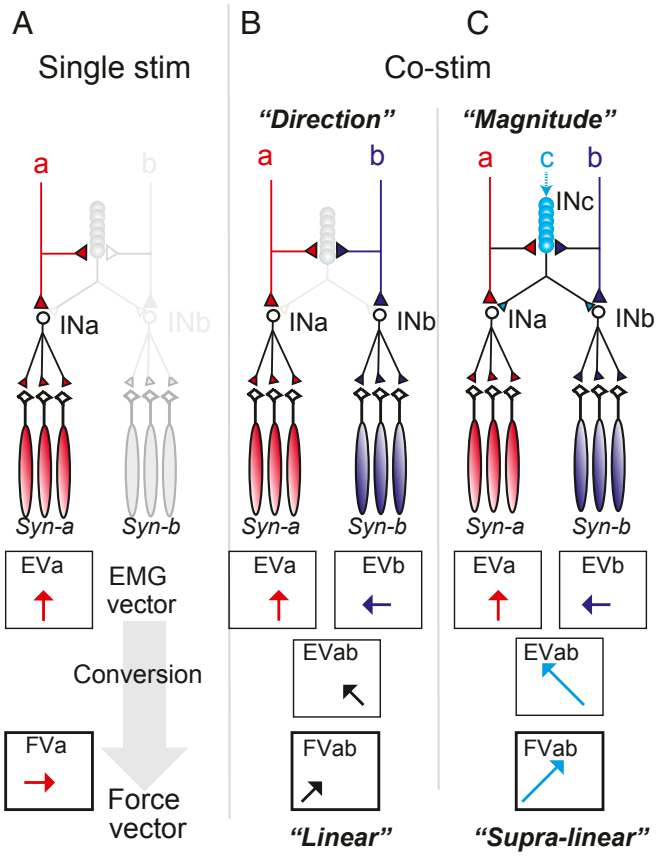

Fig. 6. Independent amplitude and direction coding of movements in the primate spinal cord: a hypothesis. (*A*) Single-site stimulation: stimulation activates interneurons (INa) and the axons of neurons projecting to them (a). As a result, motoneurons and muscles innervated by INa (Synergy-a; Syn-a) are recruited during stimulation. This muscle synergy creates a specific EMG balance within the recruited muscles, which is represented as the EMG vector (Eva; red arrow). A given EMG vector should then be transformed into the Force vector (FVa; black arrow). (*B*) Costimulation in the frog and/or lumbar spinal cord. Stimulation activates two sets of interneurons (INa and INb) and the axons of neurons projecting to both of them (a and b). As a result, motoneurons and muscles innervated by INa (Syn-a) and INb (Syn-b) are recruited, and the corresponding EMG vectors represented by Syn-a (EVa: red arrow) and Syn-b (EVb: blue arrow) are generated independently and simultaneously. Thus, the linear sum of EVa and EVb (EVab) is observed and transformed to the output force vector (FVab; black arrow). (*C*) Costimulation in the primate and/or cervical spinal cord. Stimulation activates interneurons (INa and INb) and the axons of neurons projecting to both of them (a and b). In addition, both stimuli acting in concert affect the recruitment of a separate set of interneurons (INc) as a result of spatiotemporal summation. INc is a purported group of neurons that cofacilitate INa and INb. The excitability of INa and INb can therefore both be increased equally, resulting in a supralinear output from the same inputs from a and b, whereby a larger number of motoneurons and their corresponding muscle fibers are activated. Consequently, the observed EMG vector (EVab) and force field vector (FVab) are much larger in amplitude (cyan arrow), but the direction is similar to that of the linear sum (*B*). Thus, directional control can be achieved by activating commands a and b, while separately amplitude control can be realized by independently activating command c. See *Discussion* for details.

summation being more linear in the proximal muscles (Fig. 4*E*). Therefore, both hand and arm movements are likely to be generated by the flexible combination of spinal motor modules. However, because the evidence for modular control of the proximal muscles of the primate arm is currently much more incomplete compared to that for the distal finger muscles (23–25), generation of arm movements using proximal muscle motor modules requires further investigation. Third, considering the similarity between macaque and human neuroanatomical structures (41–43), as well as their functions (44–46), our results suggest that limb movements in humans might also be generated by the combination of multiple motor modules. Interestingly, epidural stimulation of the lumbar segment in patients with spinal cord injury has been reported to recruit a small number of muscle synergies (47), and the contribution of each synergy for generating total EMG patterns was flexibly altered according to various rhythmic patterns. Moreover, neuromodulation therapies using spinal cord stimulation successfully recruited muscle synergies in the rat (48) and generated synergistic movements in human patients (49), by which we can infer the existence of spinal motor modules in humans.

Strong Supralinear Summation of Force Field Magnitude: A Unique Feature of Primate or Cervical Spinal Cord? In contrast to the force field direction vectors, we found strong supralinear summation in force field magnitudes after costimulation (Fig. 5 *A* and *D*). We also found corresponding supralinear summation in the magnitude of the EMG vectors, particularly in those of distal muscles (Fig. 5 *B*, *E*, and *H*).

Linearity in the summation of force field magnitude during costimulation has been reported in two previous studies (5, 34); both measured the force field above the ankle joint after stimulating the lumbar spinal cord. Although it was slightly larger in the cat (Table 1), both studies showed a simple linear summation of force magnitudes, which is a clear contrast with the present study. A promising clue for untangling this discrepancy is that in the current study the SI for EMG vector magnitude depended on the muscle group (Fig. 5*H*). We found similar supralinear SIs in the force field (Fig. 5*G*) and EMG vector of elbow muscles (Fig. 5*H*). In contrast, the SI for the shoulder muscle was closer to linear (mean: 0.41 $\pm$ 0.12, median: 0.09) with higher directional similarity to the simple linear sum (Fig. 4*E*). Therefore, a reasonable assumption is that we would have observed simple linear summations in both force field direction and magnitude if the force fields had been generated exclusively by the proximal, shoulder muscles. The sublinear or mostly supralinear summation of vector magnitude, as a logical consequence, can be ascribed to the action of more distal, elbow, and wrist muscles. This hypothesis of a proximal–distal bias in the nonlinearity of force field magnitude is further supported by the finding that the most distal wrist/finger muscles exhibited the greatest supralinearity of vector magnitudes by far (Fig. 5*H*). A proximal–distal bias for nonlinear magnitude can also explain the differences between previous findings and what we report here. For example, a linear sum of both the direction and magnitude of the end-point force field might indicate that this bias is less dominant either in the motor modules for leg muscles in the lumbar cord or in the frog and rodent spinal cords in general. Conversely, this proximal–distal bias could be a unique feature for either spinal modules of the cervical cord (yet to be examined in other species), the primate cord in general, or specific to the primate cervical cord.

A neural mechanism underlying the supralinear summation of magnitude is hypothesized in Fig. 6*C*. As already discussed, the direction of the EMG vector represented in each premotor neuron can be summed linearly and is indirectly correlated to the force field direction (Fig. 6*B*). However, nonlinear magnitude facilitation could be explained by supposing a large number of upstream interneurons (INc) that are shared to an equal extent by INa and INb. Costimulation might indirectly increase the excitability of INa and INb (Fig. 5 *B* and *C*) by recruiting a large number of INcs via spatial facilitation, the hallmark of the convergent spinal interneuronal system (33), thereby magnifying the activity of INa and INb proportionately and creating the observed supralinear magnification of EMG and force vectors without changing the overall directionality (either in physical space for the force field or in EMG vector space for the motor response). The nonlinear magnification during costimulation can also be expected owing to supralinear summation of EPSPs when the excitatory synaptic input to INc from both INa and INb is temporally facilitated (50, 51).

Based on this hypothesis, what is unique about the motor module for the primate or cervical cord compared with the systems previously studied? One possibility may be the larger number of interneurons like the purported INc. For example, the total number of neurons in a single spinal cord lumbar segment of the turtle was estimated at 47,504 (52), while an equivalent estimation in monkeys (*Macaca fascicularis*) is 1,920,000 (53). Therefore, the number of spinal lumbar neurons in turtles and other "lower" animals could be far less than that in macaque monkeys. Additionally, the total number of neurons (per length) in the cervical and lumbar cords seems to be comparable in the rodent (54) but is slightly larger in the cervical cord (compared with the lumbar cord) in both nonhuman primates and humans (53). Therefore, if the number of interneurons like INc in Fig. 6*C* increases in parallel with the total number of neurons in the primate cervical spinal cord, then supralinear magnitude summation (facilitation) might be expected.

What is the advantage of having supralinear summation in amplitude be unique to the distal muscles of the forelimb, especially in nonhuman primates and possibly humans? Determining how the brain and spinal cord control hand and wrist movements is challenging, primarily because of the anatomical complexity and the high DOF therein. While our finding that linear summation of force direction is conserved in the spinal cords of nonhuman primates should indicate that spinal modules can be used to simplify the process of planning hand paths in space, the spinal mechanism for the supralinear magnitude amplification can have an independent role. For example, bringing a cup of water to your mouth is achieved by the same overall kinematics whether the cup is full or empty. However, the force required to support the weight of the cup depends on how much water it contains. Separately changing the commands sent to each module is one strategy the CNS could utilize, but this requires that the coherence between modules also be maintained; otherwise, the movement kinematics will be altered. Boosting the muscle forces across an already-computed path through a separate channel of interneurons avoids this risk. Cortical coding of movement direction has been shown to occur earlier than that of movement amplitude in both primary, premotor, and parietal cortexes (55). Because most corticospinal cells from the motor and parietal cortex terminate in the intermediate spinal layer (56), we speculate that this cortical command independently controls movement amplitude and direction by activating different sets of spinal interneurons.

Finally, we must point out that differences in experimental constraints among this and previous studies (Table 1) might underlie the different levels of summation for force field magnitude among species or in different parts of the spinal cord. For example, the reduced preparation (i.e., spinalization or decerebration) could induce acute and/or chronic changes in spinal circuitry, but as a trade-off the intact preparation needs anesthesia, which affects the excitability of spinal neurons to some extent (57). Therefore, a future experiment specifically designed to evaluate multiple species or an experiment that includes interlimb comparison under a comparable setting (e.g.,

intact, nonanesthetized preparation) is needed to confirm our hypothesis.

Methods

Three male rhesus macaques (monkey TE, 4.1 kg; monkey TS, 5.0 kg; monkey NE, 10.1 kg) were used in this study. All procedures were performed in accordance with the NIH *Guide for the Care and Use of Laboratory Animals* (58) and were approved by the local ethics committee for primate research at the National Institute of Neuroscience (Japan).

Surgery. Each monkey underwent two separate surgical operations, one for implanting EMG wires in the muscles of the forelimb and one for implanting the electrode array into the cervical spinal cord. The spinal array surgery was performed 2 to 4 wk after the EMG wire surgery. During surgeries, monkeys were anesthetized (sevoflurane 1.5 to 2.5% in 2:1 O_2/N_2O) and artificially ventilated. Respiration rate was adjusted to keep end-tidal CO_2 within 30 to 35 mmHg.

EMG Implant. The skin and underlying tissue were removed from an area posterior to bregma on the skull of the monkey and a T-bolt and several small screws were inserted for use as an EMG ground and to secure the headpiece, which protruded from the dental cement. Bipolar EMG electrodes constructed from braided stainless-steel wires (AS632; Cooner Wire) were tunneled subcutaneously to their target muscles in the left arm and pulled through small puncture openings in the skin over each target muscle, and their ends were inserted into each muscle using hypodermic needles through the same puncture (59). Implant sites were confirmed by intramuscular electrical stimulation. The wire connectors were then cemented in place on top of the skull. A resin tube was added to the headpiece to support the head for later experiments in a seated position. EMG electrodes were implanted in three shoulder muscles (pectoralis major [PEC], clavicular deltoid [DEC], and spinal deltoid [DES]), four elbow muscles (biceps long head [BIC], brachioradialis [BRD], triceps long head [TRI], and the lateral head of the triceps brachii [TLA, monkeys TE and NE only]), two wrist muscles (extensor carpi radialis [ECR] and flexor carpi radialis [FCR]), and three finger muscles (adductor pollicis [ADP], flexor digitorum superficialis [FDS], and first dorsal interosseous [FDI]).

Spinal Array Implant. An incision was made along the midline of the back and the C3–T2 vertebrae were exposed bilaterally from the spinous process to the lateral masses. A laminectomy was performed from C4 to C5 and the dura matter removed to expose the dorsal surface of the spinal cord. A screw was inserted transarticularly into each lateral mass. The screws on each side were reinforced by tying them together with stainless-steel wires and then covering them with dental resin, which was allowed to set. A floating microarray electrode array (FMA; MicroProbes) was implanted. The array consisted of 12 (monkeys TS and TE) or 32 (monkey NE) shanks, which were 3 mm (monkey TS), 4 mm (monkey TE), or a mixture of 2, 3, and 4 mm (monkey NE) long. They were arranged in a 3×4 (TS, TE) or 4×8 (NE) offset grid with an intershank spacing of 7.5 mm (TS, TE) or 2.5 mm (NE). The impedance of each electrode ranged from 0.5 to 1.2 MΩ. The array was implanted in the C6–C7 region such that the effective stimulation field would excite muscles from the shoulder to the intrinsic muscles of the left arm. A rectangular chamber was cemented to the vertebrae to protect the implant connector.

Experimental Procedures. Recording sessions were performed 7 (monkey TE), 72 (monkey TS), and 49, 56, and 72 d (monkey NE, each day using different electrode depths) after FMA implantation. Before starting each recording session, monkeys were anesthetized using ketamine (initial dose: 3.0 mg/kg, intramuscularly [i.m.], supplemented at 2.3 to 3.8 mg/kg/h) and medetomidine hydrochloride (initial dose: 100 μg/kg, i.m., supplemented at 30 to 50 μg/kg/h). At this time, they were also given ketoprofen (initial dose: 3.0 mg/kg) as an additional analgesic. During all experimental procedures, the depth of anesthesia was strictly maintained by veterinary staff, who continuously monitored multiple vital signs (heart rate, respiratory rate, blood pressure, and oxygen saturation) to confirm that sufficient pain management and consistent anesthetic depth was achieved. Each monkey was laid in a prone position on a table with the left arm outstretched and the origin for the force field (0,0) defined as the sensor location closest to 20 cm left of the base of the coracoid process (Fig. 1*A*). Two padded poles were placed around the upper left (ipsilateral) arm at the shoulder joint to stabilize the position of the trunk during the experiment. The left wrist was secured just proximal to the styloid process of the radius in a specially designed swiveling U-shaped holder with an integrated multiaxis force sensor (Fig. 1*B*; Nano17; ATI Industrial Automation) and further reinforced by putting a custom-fit form inside the holder and wrapping the holder and wrist together with surgical tape (Micropore; 3M) to prevent any subtle movement of the joint within the holder due to intraspinal microsimulation. The hand distal to the U-shaped holder was kept in a neutral position without any restriction and without contacting any surface. Under this setup, the limb was immobilized above the wrist in all six DOF. We allowed limited hand and finger movement to reduce their effect on the force measured at the transducer. The U-shaped holder could then be fixed at one of seven points on a square grid with an 8-cm interval (Fig. 1*A*). Among the seven wrist positions, the joint angle was immobilized between 16.1° ± 14.2° and 74.9° ± 9.1° for the shoulder or between 46.4° ± 4.2° and 150.3° ± 24.0° for the elbow (mean ± SD for three monkeys), covering on average 42.3% (±8.7%) of the sweep area of the arm from alongside the body to perpendicular to the body, as enclosed by the wrist. The right arm and hand were fully extended and placed next to the body, parallel to the body axis. Both legs were also fully extended.

Before each recording session, we tested the threshold current required to evoke forelimb motor responses for each electrode in the FMA and selected the four FMA electrodes with the lowest thresholds. For monkey NE, different sets of four electrodes were used for the three recording days, with each set at different electrode depths (2, 3, and 4 mm). Threshold currents were defined as the minimum current necessary to induce any detectable twitch of limb and finger muscle or a measurable force at the wrist as evoked by an intraspinal microstimulation (ISMS) train of 25 biphasic (negative–positive) pulses (400-μs duration at 50 Hz) at the start of the recording day. During each recording session, the monkey's arm was manually moved through a randomly ordered series of predefined locations on a custom-designed pegboard. A single ISMS train was composed of 25 bipolar pulses (400 μs each; total time: 500 ms at 50 Hz) of current just above the threshold.

This current was 35 to 60 μA (monkey TE), 160 to 490 μA (monkey NE), or 250 to 250 μA (monkey TS). At each hand position, we repeated the following stimulus sequence six times, activating each pairwise combination of the four electrode sites recorded in that session in series: first, a 500-ms ISMS train (25 pulses) to each electrode site of each possible pair of electrodes with a 500-ms gap between each stimulation and a 3-s pause before continuing to costimulation. Then, 500-ms ISMS trains were delivered simultaneously to both sites of each possible pair, with a 3-s interval between pairs. After all six cycles through the pair combinations were completed at one wrist position, the U-shape wrist holder was moved to another point on the grid.

The output from the 500-ms ISMS to the upper limb was evaluated using both the end-point force at the wrist as well as EMG signals from the implants in the shoulder, elbow, wrist, and finger muscles. The *x* and *y* axis forces (mediolateral and anteroposterior, respectively) were recorded with a resolution of <0.01 N using an ATI Nano17 six-axis transducer. Evoked EMGs were amplified (×1,500 to 5,000) and bandpass-filtered (5 Hz to 3 kHz) using a multichannel differential amplifier (AB-611J and SS-1611; Nihon Kohden) and digitized at 10 kHz (128-channel neural signal processor, Blackrock Microsystems).

Data Analysis.

Force. The process through which the force fields generated by the ISMS were characterized at each intraspinal site is described in Fig. 1 *C–F*. The force vector at a particular location in the field was defined as the mean force amplitude and X–Y direction at the time of stimulation (Fig. 1 *C–E*). The force field composed of the different recording positions on the wrist was then interpolated using the three nearest known force vectors to obtain a more continuous field (F) (5). We defined a field *F* as a collection of force vectors sampled from *N* hand positions ($x_1 x_2 \ldots x_N$).

To assess the effect of costimulation, we compared the expected force field due to linear summation ($F_{Ex} = F_A + F_B$, where F_A and $F_B$are force fields generated by independent intraspinal stimulation to sites A and B, respectively) and the observed force field generated by simultaneous stimulation of the same two sites (F_{Ob}). We computed the directional similarity between force vectors and scaling coefficients using a method similar to that described in the original papers (1, 4, 5). We first used the definition of the total inner-product operation between two fields, defined as the sum across all inner-product operations between the two sampled force vectors in each of the N hand positions. Let $F_{Ex}(x_i)$ and $F_{Ob}(x_i)$ denote two collections of force

vectors sampled at N locations, x_1, x_2, . . . x_N. We define the inner product, $<F_{Ex}, F_{Ob}>$, between these two sampled fields as

$$\langle F_{Ex}, F_{Ob}\rangle \equiv \sum_{i=1}^{N} F_{Ex}(x_i)\cdot F_{Ob}(x_i), \quad [1]$$

where "·" stands for the ordinary inner product of two Cartesian vectors. The similarity between the fields is defined as the cosine of the angle between them—the inner product of the two fields divided by the norms of the fields, defining the norm as

$$\|F\| \equiv \langle F, F\rangle^{1/2}, \quad [2]$$

and thus the cosine similarity is the cosine of the angle between two sampled fields, F_{Ex} and F_{Ob}:

$$\text{Cosine Similarity} = \cos(F_{Ex}, F_{Ob}) \equiv \frac{\langle F_{Ex}, F_{Ob}\rangle}{\|F_{Ex}\|\cdot\|F_{Ob}\|}. \quad [3]$$

In the original work, they assumed that the field observed during dual-site stimulation would be the linear sum of the two-component fields, with maintained directionality. However, the magnitude of the field could be scaled up or down. Therefore, they defined the observed field as

$$F_{Ob} \simeq c[F_A + F_B] = c[F_{Ex}], \quad [4]$$

or, more simply, a scalar applied to the hypothesized simple linear summation of the component fields. With this definition they then were able to give the least square expression for the scaling coefficient c:

$$c = \frac{\langle F_{Ex}, F_{Ob}\rangle}{\langle F_{Ex}, F_{Ex}\rangle}, \quad [5]$$

by substituting Eq. **4** into Eq. **1**.

We also used the scaling coefficient to compare the scaling of single vectors instead of force fields. All of the equations work in the same way, with an N of 1 making the equation

$$c = \frac{\langle V_{Ex}, V_{Ob}\rangle}{\langle V_{Ex}, V_{Ex}\rangle}, \quad [5a]$$

where V_{Ex} and V_{Ob} are vectors from a specific intraspinal site combination and hand location. As noted in *Results*, the scaling coefficient c ranged from near zero (0.06) to nearly 150, with a perfect linear sum being represented by a value of 1. To have a measure that was more symmetrically distributed about this linear sum (to match the hypothesis that the resultant field would be the simple linear sum of the two component fields) and to recenter this value to zero, we defined the SI as the natural logarithm (ln) of scaling coefficient c:

$$\text{SI} = \ln(c). \quad [6]$$

In cases in which we compared force amplitude, SI was similarly calculated, with c being defined as the ratio of observed force magnitude during costimulation to the expected linear sum of magnitudes observed during single-site stimulation, and the magnitude "m" defined as

$$m = \sqrt{x^2 + y^2}, \quad [7]$$

where x and y are the means of the force responses for these axes over the course of stimulation.

EMG. After recorded EMGs were software-filtered (fourth-order Butterworth, 10 to 1,000 Hz), evoked EMG responses were identified and measured as follows. First, the background level of the signal from 30 to 10 ms before the stimulation (baseline period) was computed using all trials recorded for each intraspinal site–muscle pair and each posture; second, trials with a significant response (>3× the SD of the background signal) were selected if any peaks or troughs continuously exceeded this voltage for >1 ms within the 20 ms after stimulation onset (the detection window); third, the area of the rectified signal during the time of stimulation, excluding the time of any stimulus artifact, was calculated and used in the analysis.

To find the contribution of each muscle to force direction, we measured the correlation between EMG and force. We calculated the direction of the force vector in response to the first stimulation train in each intraspinal site and seven wrist positions, with "east" (the direction from the positioning grid toward the animal) as 0, thus force directed "north" is positive and "south" negative. We calculated the absolute correlation between the force output direction in each of the seven arm configurations for each stimulation site and the corresponding EMG magnitudes for each of the 11 muscles. Site–muscle combinations were included only if all wrist positions exhibited a significant response.

EMG field. To assess the effect of costimulation on muscle activation so that it would be comparable to the effect on force fields, we defined EMG "fields" across the possible arm configurations for a group of M muscles as a collection of M-dimensional vectors in N hand positions ($x_1 x_2 \ldots x_N$), with each value in the vectors corresponding to the mean magnitude of the response to the first stimulation train for one muscle. For example, the "elbow" group comprised four muscles (BIC, BRD, TLA, and TLN), thus generating an EMG field with four-dimensional vectors. The values of each vector corresponded to the mean magnitude of responses in each respective muscle. This group of vectors representing muscle output at the various arm configurations was then used to calculate the similarity and SIs using the same equations that were used to calculate the force fields.

To estimate the chance level for a given group, we applied a bootstrap analysis by picking sets of muscles at random for each position in the grid (and varying the selected random muscles between the two costimulated sites and across the grid). This analysis was repeated 10,000 times for each dimensional size. For example, we bootstrap selected two random muscles to match the vector size of the top-two muscle group, and we selected 12 muscles for the full vector. This generated a range of chance-level similarities for comparison. We set the 95th percentile of this distribution as the significance limit. Therefore, if the cosine similarity was higher than 9,500 of the similarities calculated using the same number of randomly selected muscles, we concluded that it was higher than what was expected by chance. Because the chance level varied depending on the numbers of muscles, when we compared muscle groups composed of different numbers of muscles, we subtracted from each of the groups the mean chance level for the appropriate number of muscles and then applied the stated statistical test.

Data Availability. All study data are included in the paper and *SI Appendix*.

ACKNOWLEDGMENTS. This work was supported by grants-in-aid for scientific research from the Ministry of Education, Culture, Sports, Science and Technology of Japan (18020030, 18047027, 26120003, 19K21825, 19H05724, and 19H01092 to K.S. and 19H03975 and 19H05311 to T.T.), the Japan Science Technology Agency Precursory Research for Embryonic Science and Technology program (to K.S.), and the Uehara Memorial Foundation, the Naito Foundation, and the Takeda Science Foundation (to T.T.). D.K. was a Japan Society for the Promotion of Science summer fellow supported by NSF Grant OISE-1108063. We thank C. Sasaki for technical assistance, Jeehee Kim for helping with surgery, Michel Lemay for lending the multiaxis force sensor, and Tomomichi Oya and Jonas Zimmermann for helping with some surgery and recording. We also thank Adam Phillips, PhD for editing a draft of this manuscript.

1. E. Bizzi, F. A. Mussa-Ivaldi, S. Giszter, Computations underlying the execution of movement: A biological perspective. *Science* **253**, 287–291 (1991).
2. E. Bizzi, V. C. Cheung, A. d'Avella, P. Saltiel, M. Tresch, Combining modules for movement. *Brain Res. Brain Res. Rev.* **57**, 125–133 (2008).
3. S. F. Giszter, Motor primitives–New data and future questions. *Curr. Opin. Neurobiol.* **33**, 156–165 (2015).
4. S. F. Giszter, F. A. Mussa-Ivaldi, E. Bizzi, Convergent force fields organized in the frog's spinal cord. *J. Neurosci.* **13**, 467–491 (1993).
5. F. A. Mussa-Ivaldi, S. F. Giszter, E. Bizzi, Linear combinations of primitives in vertebrate motor control. *Proc. Natl. Acad. Sci. U.S.A.* **91**, 7534–7538 (1994).
6. A. d'Avella, E. Bizzi, Low dimensionality of supraspinally induced force fields. *Proc. Natl. Acad. Sci. U.S.A.* **95**, 7711–7714 (1998).
7. E. Bizzi, A. D'Avella, P. Saltiel, M. Tresch, Modular organization of spinal motor systems. *Neuroscientist* **8**, 437–442 (2002).
8. M. A. Lemay, J. E. Galagan, N. Hogan, E. Bizzi, Modulation and vectorial summation of the spinalized frog's hindlimb end-point force produced by intraspinal electrical stimulation of the cord. *IEEE Trans. Neural Syst. Rehabil. Eng.* **9**, 12–23 (2001).
9. P. Saltiel, K. Wyler-Duda, A. d'Avella, R. J. Ajemian, E. Bizzi, Localization and connectivity in spinal interneuronal networks: The adduction-caudal extension-flexion rhythm in the frog. *J. Neurophysiol.* **94**, 2120–2138 (2005).
10. P. Saltiel, K. Wyler-Duda, A. D'Avella, M. C. Tresch, E. Bizzi, Muscle synergies encoded within the spinal cord: Evidence from focal intraspinal NMDA iontophoresis in the frog. *J. Neurophysiol.* **85**, 605–619 (2001).
11. M. C. Tresch, E. Bizzi, Responses to spinal microstimulation in the chronically spinalized rat and their relationship to spinal systems activated by low threshold cutaneous stimulation. *Exp. Brain Res.* **129**, 401–416 (1999).
12. V. Caggiano, V. C. Cheung, E. Bizzi, An optogenetic demonstration of motor modularity in the mammalian spinal cord. *Sci. Rep.* **6**, 35185 (2016).

13. M. A. Lemay, W. M. Grill, Modularity of motor output evoked by intraspinal microstimulation in cats. *J. Neurophysiol.* **91**, 502–514 (2004).
14. A. d'Avella, L. Fernandez, A. Portone, F. Lacquaniti, Modulation of phasic and tonic muscle synergies with reaching direction and speed. *J. Neurophysiol.* **100**, 1433–1454 (2008).
15. E. J. Perreault, K. Chen, R. D. Trumbower, G. Lewis, Interactions with compliant loads alter stretch reflex gains but not intermuscular coordination. *J. Neurophysiol.* **99**, 2101–2113 (2008).
16. M. Santello, G. Baud-Bovy, H. Jörntell, Neural bases of hand synergies. *Front. Comput. Neurosci.* **7**, 23 (2013).
17. Y. P. Ivanenko, R. E. Poppele, F. Lacquaniti, Five basic muscle activation patterns account for muscle activity during human locomotion. *J. Physiol.* **556**, 267–282 (2004).
18. S. A. Safavynia, G. Torres-Oviedo, L. H. Ting, Muscle synergies: Implications for clinical evaluation and rehabilitation of movement. *Top. Spinal Cord Inj. Rehabil.* **17**, 16–24 (2011).
19. L. Dipietro *et al*., Changing motor synergies in chronic stroke. *J. Neurophysiol.* **98**, 757–768 (2007).
20. P. K. Artemiadis, K. J. Kyriakopoulos, EMG-based control of a robot arm using low-dimensional embeddings. *IEEE Trans. Robot.* **26**, 393–398 (2010).
21. C. Alessandro, I. Delis, F. Nori, S. Panzeri, B. Berret, Muscle synergies in neuroscience and robotics: From input-space to task-space perspectives. *Front. Comput. Neurosci.* **7**, 43 (2013).
22. H. Pham *et al*., Extraction and implementation of muscle synergies in neuromechanical control of upper limb movement. *Adv. Robot.* **28**, 745–757 (2014).
23. T. Takei, K. Seki, Spinal interneurons facilitate coactivation of hand muscles during a precision grip task in monkeys. *J. Neurosci.* **30**, 17041–17050 (2010).
24. T. Takei, K. Seki, Spinal premotor interneurons mediate dynamic and static motor commands for precision grip in monkeys. *J. Neurosci.* **33**, 8850–8860 (2013).
25. T. Takei, J. Confais, S. Tomatsu, T. Oya, K. Seki, Neural basis for hand muscle synergies in the primate spinal cord. *Proc. Natl. Acad. Sci. U.S.A.* **114**, 8643–8648 (2017).
26. S. A. Overduin, A. d'Avella, J. M. Carmena, E. Bizzi, Microstimulation activates a handful of muscle synergies. *Neuron* **76**, 1071–1077 (2012).
27. S. L. Amundsen Huffmaster, G. M. Van Acker 3rd, C. W. Luchies, P. D. Cheney, Muscle synergies obtained from comprehensive mapping of the primary motor cortex forelimb representation using high-frequency, long-duration ICMS. *J. Neurophysiol.* **118**, 455–470 (2017).
28. S. L. Amundsen Huffmaster, G. M. Van Acker 3rd, C. W. Luchies, P. D. Cheney, Muscle synergies obtained from comprehensive mapping of the cortical forelimb representation using stimulus triggered averaging of EMG activity. *J. Neurosci.* **38**, 8759–8771 (2018).
29. S. S. Chan, D. W. Moran, Computational model of a primate arm: From hand position to joint angles, joint torques and muscle forces. *J. Neural Eng.* **3**, 327–337 (2006).
30. I. Kurtzer, J. A. Pruszynski, T. M. Herter, S. H. Scott, Primate upper limb muscles exhibit activity patterns that differ from their anatomical action during a postural task. *J. Neurophysiol.* **95**, 493–504 (2006).
31. S. Giszter, V. Patil, C. Hart, Primitives, premotor drives, and pattern generation: A combined computational and neuroethological perspective. *Prog. Brain Res.* **165**, 323–346 (2007).
32. A. d'Avella, A. Portone, L. Fernandez, F. Lacquaniti, Control of fast-reaching movements by muscle synergy combinations. *J. Neurosci.* **26**, 7791–7810 (2006).
33. F. Baldissera, H. Hultborn, M. Illert, "Integration in spinal neuronal systems" in *Handbook of Physiology*, V. B. Brooks, Ed. (American Physiological Society, Bethesda, MD, 1981), Vol. vol. II, pp. 509–595.
34. M. A. Lemay, D. Grasse, W. M. Grill, Hindlimb endpoint forces predict movement direction evoked by intraspinal microstimulation in cats. *IEEE Trans. Neural Syst. Rehabil. Eng.* **17**, 379–389 (2009).
35. D. S. Soteropoulos, S. A. Edgley, S. N. Baker, Spinal commissural connections to motoneurons controlling the primate hand and wrist. *J. Neurosci.* **33**, 9614–9625 (2013).
36. E. Jankowska, S. A. Edgley, P. Krutki, I. Hammar, Functional differentiation and organization of feline midlumbar commissural interneurones. *J. Physiol.* **565**, 645–658 (2005).
37. W. J. Kargo, S. F. Giszter, Rapid correction of aimed movements by summation of force-field primitives. *J. Neurosci.* **20**, 409–426 (2000).
38. W. J. Kargo, S. F. Giszter, Individual premotor drive pulses, not time-varying synergies, are the units of adjustment for limb trajectories constructed in spinal cord. *J. Neurosci.* **28**, 2409–2425 (2008).
39. C. B. Hart, S. F. Giszter, A neural basis for motor primitives in the spinal cord. *J. Neurosci.* **30**, 1322–1336 (2010).
40. A. J. Levine *et al*., Identification of a cellular node for motor control pathways. *Nat. Neurosci.* **17**, 586–593 (2014).
41. M. Petrides, D. N. Pandya, Dorsolateral prefrontal cortex: Comparative cytoarchitectonic analysis in the human and the macaque brain and corticocortical connection patterns. *Eur. J. Neurosci.* **11**, 1011–1036 (1999).
42. M. Petrides, D. N. Pandya, Comparative cytoarchitectonic analysis of the human and the macaque ventrolateral prefrontal cortex and corticocortical connection patterns in the monkey. *Eur. J. Neurosci.* **16**, 291–310 (2002).
43. P. L. Croxson *et al*., Quantitative investigation of connections of the prefrontal cortex in the human and macaque using probabilistic diffusion tractography. *J. Neurosci.* **25**, 8854–8866 (2005).
44. G. Rees, K. Friston, C. Koch, A direct quantitative relationship between the functional properties of human and macaque V5. *Nat. Neurosci.* **3**, 716–723 (2000).
45. M. Koyama *et al*., Functional magnetic resonance imaging of macaque monkeys performing visually guided saccade tasks: Comparison of cortical eye fields with humans. *Neuron* **41**, 795–807 (2004).
46. M. Petrides, G. Cadoret, S. Mackey, Orofacial somatomotor responses in the macaque monkey homologue of Broca's area. *Nature* **435**, 1235–1238 (2005).
47. S. M. Danner *et al*., Human spinal locomotor control is based on flexibly organized burst generators. *Brain* **138**, 577–588 (2015).
48. N. Wenger *et al*., Spatiotemporal neuromodulation therapies engaging muscle synergies improve motor control after spinal cord injury. *Nat. Med.* **22**, 138–145 (2016).
49. S. Sasada *et al*., Volitional walking via upper limb muscle-controlled stimulation of the lumbar locomotor center in man. *J. Neurosci.* **34**, 11131–11142 (2014).
50. H. Urakubo, T. Aihara, S. Kuroda, M. Watanabe, S. Kondo, Spatial localization of synapses required for supralinear summation of action potentials and EPSPs. *J. Comput. Neurosci.* **16**, 251–265 (2004).
51. J. S. Nettleton, W. J. Spain, Linear to supralinear summation of AMPA-mediated EPSPs in neocortical pyramidal neurons. *J. Neurophysiol.* **83**, 3310–3322 (2000).
52. S. Walløe, U. V. Nissen, R. W. Berg, J. Hounsgaard, B. Pakkenberg, Stereological estimate of the total number of neurons in spinal segment D9 of the red-eared turtle. *J. Neurosci.* **31**, 2431–2435 (2011).
53. J. Bahney, C. S. von Bartheld, The cellular composition and glia-neuron ratio in the spinal cord of a human and a nonhuman primate: Comparison with other species and brain regions. *Anat. Rec.* **301**, 697–710 (2018).
54. R. Bjugn, H. J. Gundersen, Estimate of the total number of neurons and glial and endothelial cells in the rat spinal cord by means of the optical disector. *J. Comp. Neurol.* **328**, 406–414 (1993).
55. K. Hadjidimitrakis *et al*., Common neural substrate for processing depth and direction signals for reaching in the monkey medial posterior parietal cortex. *Cereb. Cortex* **24**, 1645–1657 (2014).
56. M. P. Galea, I. Darian-Smith, Multiple corticospinal neuron populations in the macaque monkey are specified by their unique cortical origins, spinal terminations, and connections. *Cereb. Cortex* **4**, 166–194 (1994).
57. N. el-Yassir, S. M. Fleetwood-Walker, A 5-HT1-type receptor mediates the antinociceptive effect of nucleus raphe magnus stimulation in the rat. *Brain Res.* **523**, 92–99 (1990).
58. National Research Council, *Guide for the Care and Use of Laboratory Animals*, (National Academies Press, Washington, DC, 8th Ed., 2011).
59. M. C. Park, A. Belhaj-Saïf, P. D. Cheney, Chronic recording of EMG activity from large numbers of forelimb muscles in awake macaque monkeys. *J. Neurosci. Methods* **96**, 153–160 (2000).
60. H. Yaguchi *et al*., Modulation of spinal motor output by initial arm postures in anesthetized monkeys. *J. Neurosci.* **35**, 6937–6945 (2015).